

Analysis of $B_c \rightarrow \tau \nu_\tau$ at CEPC

Taifan Zheng¹, Ji Xu², Lu Cao³, Dan Yu⁴, Wei Wang², Soeren Prell⁵, Yeuk-Kwan E. Cheung¹, and Manqi Ruan^{4 a}

¹ School of Physics, Nanjing University, Nanjing, China

² INPAC, SKLPPC, MOE KLPPC, School of Physics and Astronomy, Shanghai Jiao Tong University, Shanghai, China

³ Physikalisches Institut der Rheinischen Friedrich-Wilhelms-Universität Bonn, 53115 Bonn, Germany

⁴ Institute of High Energy Physics, Beijing, China

⁵ Department of Physics and Astronomy, Iowa State University, Ames, IA, USA

Received: date / Revised version: date

Abstract. The precise determination of the $B_c \rightarrow \tau \nu_\tau$ branching ratio provides an advantageous opportunity for understanding the electroweak structure of the Standard Model, measuring the CKM matrix element $|V_{cb}|$ and probing new physics models. In this paper, we discuss the potential of measuring the processes of $B_c \rightarrow \tau \nu_\tau$ with τ decaying leptonically at the proposed Circular Electron Positron Collider (CEPC). We conclude that during the Z pole operation, the channel signal can achieve five σ significance with $\sim 10^9$ Z decays, and the signal strength accuracies for $B_c \rightarrow \tau \nu_\tau$ can reach around 1% level at the nominal CEPC Z pole statistics of one trillion Z decays assuming the total $B_c \rightarrow \tau \nu_\tau$ yield is 3.6×10^6 . Our theoretical analysis indicates the accuracy could provide a strong constraint on the general effective Hamiltonian for the $b \rightarrow c \tau \nu$ transition. If the total B_c yield can be determined to $\mathcal{O}(1\%)$ level of accuracy in the future, these results also imply $|V_{cb}|$ could be measured up to $\mathcal{O}(1\%)$ level of accuracy.

PACS. PACS-key describing text of that key – PACS-key describing text of that key

1 Introduction

Weak decays of heavy mesons not only provide a unique platform to test the electroweak structures of the Standard Model (SM) but can also shed light on new physics (NP) beyond the SM. Among different species of heavy mesons, the B_c^{+1} meson, discovered in 1998 by the CDF collaboration [1, 2], is of particular interest in this regard. The B_c^+ meson has specific production and decay mechanisms, and accordingly the measurement of its mass, lifetime and decay branching ratios would help to probe the underlining quark dynamics and determine SM parameters.

Consisting of two heavy quarks of different types, the B_c^+ meson has three decay categories: 1) b -quark decay with spectator c -quark; 2) c -quark decay with spectator b -quark; 3) annihilation process (e.g. $B_c^+ \rightarrow \tau^+ \nu_\tau, c\bar{s}$). The purely leptonic decay through the annihilation process is sensitive to the decay constant f_{B_c} and the CKM matrix element $|V_{cb}|$. Such a scheme has been used for the determination of $|V_{cd}|$ and $|V_{cs}|$ in $D^+/D_s^+ \rightarrow \tau^+ \nu_\tau, \mu^+ \nu_\mu$ [3]. For $|V_{cb}|$, since the $B_c^+ \rightarrow \tau^+ \nu_\tau$ channel has not been discovered, it is measured using inclusive semileptonic $b \rightarrow c$ transitions and the exclusive channel of $\bar{B} \rightarrow D^* l \bar{\nu}_l$. However, even if $B_c^+ \rightarrow \tau^+ \nu_\tau$ had been discovered, the decay $\bar{B} \rightarrow D^* l \bar{\nu}_l$ would still provide a more precise $|V_{cb}|$ measurement.

In recent years a few discrepancies have been found between the SM predictions and different experimental measurements in the bottom sector, especially in taonic decay modes of B mesons [4–6]. In view of no clear signal in the direct searches of NP to date, the implications in low-energy processes are of great importance. The study of taonic decay modes of B mesons, mostly $B \rightarrow D^{(*)} \tau \nu$ decays, have indicated some hints for lepton flavor universality violation. While these decay modes are very sensitive to vector/axial-vector type interactions, the (pseudo)scalar type interactions which can be induced in many popular NP models, e.g., the two-Higgs doublet and leptoquark models are less constrained by them. Due to the mass hierarchy $m_\tau \ll m_{B_c}$ that results in helicity suppression for $B_c^+ \rightarrow \tau^+ \nu_\tau$ with $V - A$ interactions in the SM, $B_c \rightarrow \tau \nu$ has a better sensitivity to the (pseudo)scalar NP interactions [7, 8]. Therefore, measurement of the branching ratio $\mathcal{B}(B_c^+ \rightarrow \tau^+ \nu_\tau)$ can be a key in the search for NP. As we will show in Section II, based on the current knowledge, NP can affect $\mathcal{B}(B_c^+ \rightarrow \tau^+ \nu_\tau)$ significantly, which highlights the study of this quantity in the future.

The recently proposed CEPC (Circular Electron Positron Collider) [9] provides an excellent opportunity to measure $\mathcal{B}(B_c^+ \rightarrow \tau^+ \nu_\tau)$. It has a circumference of 100 km and two interaction points. Its primary objective is the precision Higgs study at a center-of-mass-energy (\sqrt{s}) of 240 GeV with a nominal production of 10^6 Higgs. In addition, a dedicated WW threshold scan ($\sqrt{s} = 158 - 172$ GeV) and the Z factory mode ($\sqrt{s} = 91.2$ GeV) will be operated for electroweak and flavor physics studies. The Z factory will produce up to one trillion Z bosons

Send offprint requests to:

^a Email: manqi.ruan@ihep.ac.cn

¹ The charge conjugate state is implied throughout the paper.

(Tera-Z) in two years, far exceeding LEP's production [10]. Such a huge data sample will enable high precision tests of the SM and allow to study many previously unobservable processes. Furthermore, the clean e^+e^- collision environment and the well-defined initial state compared to hadron colliders are advantages for this analysis at the CEPC. (Super) B factories operating at the $\Upsilon(4S)$ center-of-mass-energy are below the energy threshold for B_c^+ production. A detailed discussion on the various advantages and prospects on flavor studies at CEPC can be found in [9].

In this paper, we discuss the potential of measuring the processes of $B_c^+ \rightarrow \tau^+ \nu_\tau$, $\tau^+ \rightarrow e^+ \nu_e \bar{\nu}_\tau$ and $\tau^+ \rightarrow \mu^+ \nu_\mu \bar{\nu}_\tau$ in $Z \rightarrow b\bar{b}$ at the CEPC. Important backgrounds are other $Z \rightarrow c\bar{c}$ and $Z \rightarrow b\bar{b}$, especially the decay of $B^+ \rightarrow \tau^+ \nu_\tau$ in $Z \rightarrow b\bar{b}$ events². Both B_c^+ and B^+ have similar masses and event topologies [3]. The main difference is the lifetime (the B_c^+ lifetime is around one third of the B^+ lifetime). The L3 experiment at LEP had originally searched for $B^+ \rightarrow \tau^+ \nu_\tau$ in 1997 with $1.475 \times 10^6 Z \rightarrow q\bar{q}$ events [11], and determined $\mathcal{B}(B^+ \rightarrow \tau^+ \nu_\tau) < 5.7 \times 10^{-4}$ at 90% CL. The study did not consider the contribution from $B_c^+ \rightarrow \tau^+ \nu_\tau$. However, [12, 13] later argued the $B_c^+ \rightarrow \tau^+ \nu_\tau$ contribution could be comparable to the $B^+ \rightarrow \tau^+ \nu_\tau$ contribution, and that a similar analysis method could be used to measure $B_c^+ \rightarrow \tau^+ \nu_\tau$. Understanding the $B^+ \rightarrow \tau^+ \nu_\tau$ background is crucial in this analysis.

We estimate the $B_c^+/B^+ \rightarrow \tau^+ \nu_\tau$ event yield at the CEPC Z pole as follows. The number of $B^+ \rightarrow \tau^+ \nu_\tau$ events produced is given by:

$$N(B^\pm \rightarrow \tau^\pm \nu_\tau) = N_Z \times \mathcal{B}(Z \rightarrow b\bar{b}) \times 2 \times f(\bar{b} \rightarrow B^+ X) \times \mathcal{B}(B^+ \rightarrow \tau^+ \nu_\tau), \quad (1)$$

where N_Z is the total number of Z bosons produced. The factor two accounts for the quark anti-quark pair. The branching ratios $\mathcal{B}(Z \rightarrow b\bar{b}) = 0.1512 \pm 0.0005$, $f(\bar{b} \rightarrow B^+ X) = 0.408 \pm 0.007$, and $\mathcal{B}(B^+ \rightarrow \tau^+ \nu_\tau) = (1.09 \pm 0.24) \times 10^{-4}$ are taken from [3]. For the B_c production, the theoretical result at next-to-leading order in α_s gives $\mathcal{B}(Z \rightarrow B_c^\pm X) = 7.9 \times 10^{-5}$ [14], and our estimate of $\mathcal{B}(B_c^+ \rightarrow \tau^+ \nu_\tau)$ (see the next section) is $(2.36 \pm 0.19)\%$. These numbers give

$$R_{B_c/B} = \frac{N(B_c^\pm \rightarrow \tau^\pm \nu_\tau)}{N(B^\pm \rightarrow \tau^\pm \nu_\tau)} = 0.28 \pm 0.05, \quad (2)$$

where we use $R_{B_c/B}$ to denote the ratio. Note that the actual uncertainty for $R_{B_c/B}$ is larger since we lack the uncertainty for $\mathcal{B}(Z \rightarrow B_c^\pm X)$. We conduct our analysis with 10^9 simulated Z boson decays including $(1.3 \pm 0.3) \times 10^4 B^\pm \rightarrow \tau^\pm \nu_\tau$ events. For simplicity and a larger signal dataset for analysis, we assume both $N(B_c^\pm/B^\pm \rightarrow \tau^\pm \nu_\tau)$ are equal to 1.3×10^4 and discuss other scenarios at the end, since the results are easily scalable for different values of $R_{B_c/B}$.

The rest of this paper is organized as follows. Sect. 2 gives the decay width of $B_c^+ \rightarrow \tau^+ \nu_\tau$ in the SM and estimates the effects in NP scenarios. Sect. 3 introduces the detector, software and the MC-simulated event samples. Sect. 4 presents the analysis method and results. The conclusion is given in Sect. 5.

² Throughout the paper, all of the $B_c^+/B^+ \rightarrow \tau^+ \nu_\tau$ events are implied to be $Z \rightarrow b\bar{b}$ events containing such decays, unless specified otherwise.

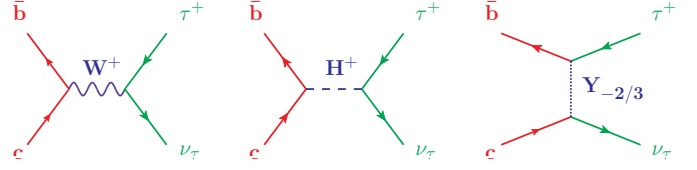


Fig. 1: Feynman diagrams for tauonic B_c decays in the SM, 2HDM and LQ models.

2 $B_c^+ \rightarrow \tau^+ \nu_\tau$ in the SM and in NP models

In the SM, the decay width of the purely leptonic decay $B_c^+ \rightarrow l^+ \nu_l$ is given by:

$$\Gamma_{\text{SM}}(B_c^+ \rightarrow l^+ \nu_l) = \frac{G_F^2}{8\pi} |V_{cb}|^2 f_{B_c}^2 m_{B_c} m_l^2 \left(1 - \frac{m_l^2}{m_{B_c}^2}\right)^2, \quad (3)$$

where G_F is the Fermi coupling constant, V_{cb} is the CKM matrix element, f_{B_c} is the decay constant, and m_{B_c} , m_l are the masses of the meson and the charged lepton, respectively. Due to helicity suppression, the τ final state has the largest branching fraction. The measurement of $B_c^+ \rightarrow \tau^+ \nu_\tau$ would help to determine the fundamental parameter $|V_{cb}|$, once the decay constant is known from first-principle calculations, i.e. lattice QCD. Feynman diagram for $B_c^+ \rightarrow \tau^+ \nu_\tau$ in the SM is shown in the left panel of Fig. 1.

With the decay constant $f_{B_c} = (0.434 \pm 0.015) \text{ GeV}$ [15], $\tau(B_c) = (0.510 \pm 0.009) \times 10^{-12} \text{ s}$ and $|V_{cb}| = (42.2 \pm 0.8) \times 10^{-3}$ [3], we obtain

$$\mathcal{B}(B_c^+ \rightarrow \tau^+ \nu_\tau) = (2.36 \pm 0.19)\%, \quad (4)$$

where the errors from the decay constant and lifetime of the B_c^+ have been added in quadrature. The uncertainty in the B_c^+ branching fraction is dominated by the decay constant that might be further reduced in a more accurate Lattice QCD calculation in the future. Other theoretical studies on the subject of B_c^+ decay can be found in [16].

Since the tau lepton has the largest mass compared to the other two species of leptons, the NP coupling might have a more evident effect in tauonic decays of heavy mesons. Two popular NP models include the two Higgs doublet model (2HDM) with a charged Higgs boson propagator similar to the W boson propagator, and the leptoquark (LQ) models that couple leptons with quarks. The charged Higgs boson in 2HDM can have a significant coupling with the tau, and thereby its contributions to decay widths could be sizable [17, 18].

Theoretical studies of NP contributions can be conducted in two distinct ways. One is to confront the explicit model predictions one by one with available experimental constraints, while the other is to employ an effective field theory (EFT) approach. Integrating out the massive particles, e.g. charged Higgs particle or the LQ in Fig. 1, the NP contributions are incorporated into a few effective operators, with the interaction strengths embedded in Wilson coefficients. A general effective Hamiltonian

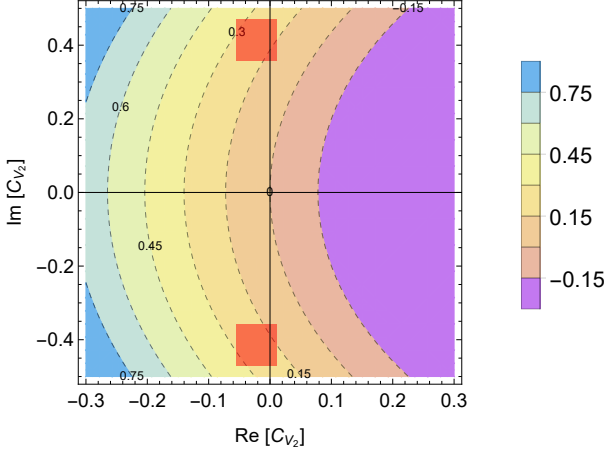


Fig. 2: Sensitivities of $(\Gamma_{\text{eff}} - \Gamma_{\text{SM}})/\Gamma_{\text{SM}}(100\%)$ to C_{V_2} . The SM lies at the origin with $\text{Re}[C_{V_2}] = \text{Im}[C_{V_2}] = 0$. Labels (in units of 100%) on contours denote the modification of branching ratios (decay widths) with respect to the SM values. The red shaded area corresponds to the global fitted results of available data on $b \rightarrow c\tau\nu$ decays, as shown in Eq. (9). These areas deviate from the SM predictions by about a few σ .

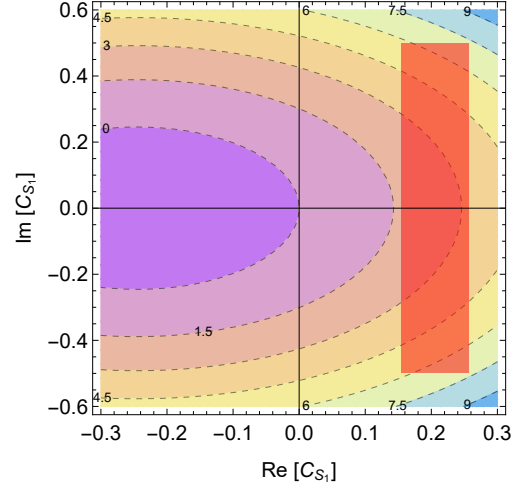


Fig. 3: Sensitivities of $(\Gamma_{\text{eff}} - \Gamma_{\text{SM}})/\Gamma_{\text{SM}}(100\%)$ to C_{S_1} . The SM lies at the origin with $\text{Re}[C_{S_1}] = \text{Im}[C_{S_1}] = 0$. Labels (in units of 100%) on contours denote the modification of branching ratios (decay widths) with respect to the SM values. The red shaded area corresponds to the global fitted results of available data on $b \rightarrow c\tau\nu$ decays, as shown in Eq. (10).

for the $b \rightarrow c\tau\nu$ transition can be written as

$$\mathcal{H}_{\text{eff}} = \frac{4G_F}{\sqrt{2}} V_{cb} [(1 + C_{V_1}) O_{V_1} + C_{V_2} O_{V_2} + C_{S_1} O_{S_1} + C_{S_2} O_{S_2}] + \text{h.c.}, \quad (5)$$

where O_i are four-fermion operators and C_i are the corresponding Wilson coefficients. The four-fermion operators are defined as

$$\begin{aligned} O_{V_1} &= (\bar{c}_L \gamma^\mu b_L) (\bar{\tau}_L \gamma_\mu \nu_L), \\ O_{V_2} &= (\bar{c}_R \gamma^\mu b_R) (\bar{\tau}_L \gamma_\mu \nu_L), \\ O_{S_1} &= (\bar{c}_L b_R) (\bar{\tau}_R \nu_L), \\ O_{S_2} &= (\bar{c}_R b_L) (\bar{\tau}_R \nu_L). \end{aligned} \quad (6)$$

where O_{V_1} is the only operator present in the SM. The 2HDM can contribute to O_{S_1} , while the LQs can have more versatile contributions depending on their spin and chirality in couplings.

Having Eq.(5) and Eq.(6) at hand, one arrives at

$$\frac{\Gamma_{\text{eff}}(B_c^+ \rightarrow \tau^+ \nu_\tau)}{\Gamma_{\text{SM}}(B_c^+ \rightarrow \tau^+ \nu_\tau)} = \left| 1 + C_{V_1} - C_{V_2} + C_{S_1} \frac{m_{B_c}^0}{m_\ell} - C_{S_2} \frac{m_{B_c}^0}{m_\ell} \right|^2, \quad (7)$$

where $m_{B_c}^0 \equiv m_{B_c}^2/(m_b + m_c)$. This expression shows the deviation of decay width of $B_c^+ \rightarrow \tau^+ \nu_\tau$ compared with the SM.

Inspired by the experimental measurements of $B \rightarrow D^{(*)} \tau \nu$ and other decays induced by $b \rightarrow c\tau\nu$, quite a few theoretical analyses of NP contributions have been made in recent years. In this work, we will make use of the results for the Wilson

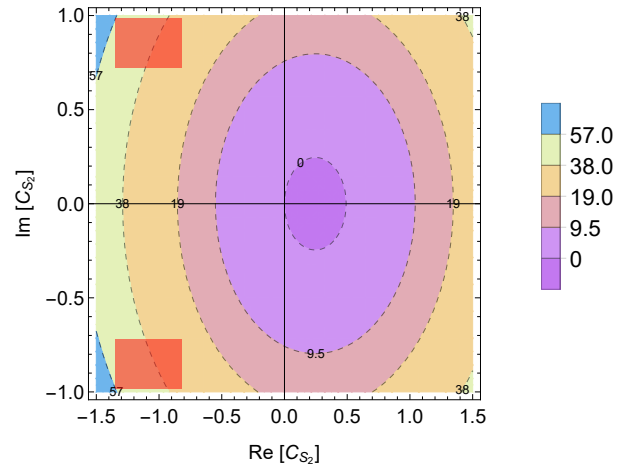


Fig. 4: Similar to Fig. 3 with red shaded area as parameter space of C_{S_2} given in Eq. (11).

coefficients from Refs.[19, 20]:

$$|1 + \text{Re}[C_{V_1}]|^2 + |\text{Im}[C_{V_1}]|^2 = 1.189 \pm 0.037, \quad (8)$$

$$C_{V_2} = (-0.022 \pm 0.033) \pm (0.414 \pm 0.056)i, \quad (9)$$

$$C_{S_1} = (0.206 \pm 0.051) + (0.000 \pm 0.499)i, \quad (10)$$

$$C_{S_2} = (-1.085 \pm 0.264) \pm (0.852 \pm 0.132)i, \quad (11)$$

and the masses:

$$\begin{aligned} m_{B_c} &= 6.2749 \text{ GeV}, & m_b &= 4.18 \text{ GeV}, \\ m_c &= 1.27 \text{ GeV}, & m_\tau &= 1.77686 \text{ GeV}. \end{aligned} \quad (12)$$

Eq. (8) directly implies that the branching fraction of $B_c^+ \rightarrow \tau^+ \nu_\tau$ can be affected by $(18.9 \pm 3.7)\%$ if only the SM-like $V-A$ operator O_{V_1} is included. If O_{V_2} is considered, the contributions to $(\Gamma_{\text{eff}} - \Gamma_{\text{SM}})/\Gamma_{\text{SM}}$ are shown in Fig. 2. The red shaded area in this figure corresponds to the global fitted results of data on B meson decays induced by $b \rightarrow c \tau \nu$, as shown in Eq. (9). In this figure and the following ones, we do not consider the correlation between the real and imaginary part in the Wilson coefficients. Two branches are found due to the ambiguous sign in the imaginary part of C_{V_2} . From this figure, one can infer that the NP contributions range from about 10% to 30%. In these two scenarios, branching fractions of $B_c^+ \rightarrow \tau^+ \nu_\tau$ are mildly affected due to helicity suppression.

If we switch to O_{S_1} , the results are shown in Fig. 3, and again the red shaded area corresponds to the global fitted results shown in Eq. (10). Similar results are shown in Fig. 4 for O_{S_2} . In these two figures, one can clearly see that $\Gamma(B_c^+ \rightarrow \tau^+ \nu_\tau)$ is dramatically affected by NP contributions. At this stage the errors do not allow a very conclusive result on the existence of NP, and accordingly measurements of this width at CEPC would help to confirm or rule out these NP scenarios.

Next let's consider the $|V_{cb}|$ measurement in the SM scenario. Its uncertainty can be derived from the relative uncertainty of the signal strength $\sigma(\mu)/\mu$. The signal strength μ is the ratio between the measured effective cross section and the corresponding SM prediction, and $\sigma(\mu)$ is its uncertainty. Therefore it is straightforward that:

$$\begin{aligned} \frac{\sigma(\mu)}{\mu} &= \frac{\sigma(N(B_c^\pm \rightarrow \tau \nu_\tau))}{N(B_c^\pm \rightarrow \tau \nu_\tau)} = \frac{\sigma(\mathcal{B}(Z \rightarrow B_c^\pm X) \mathcal{B}(B_c^+ \rightarrow \tau^+ \nu_\tau))}{\mathcal{B}(Z \rightarrow B_c^\pm X) \mathcal{B}(B_c^+ \rightarrow \tau^+ \nu_\tau)} \\ &= \frac{\sigma(\mathcal{B}(Z \rightarrow B_c^\pm) \Gamma_{\text{SM}}(B_c^+ \rightarrow \tau^+ \nu_\tau) / \Gamma(B_c^+))}{\mathcal{B}(Z \rightarrow B_c^\pm) \Gamma_{\text{SM}}(B_c^+ \rightarrow \tau^+ \nu_\tau) / \Gamma(B_c^+)}, \end{aligned} \quad (13)$$

where $\Gamma(B_c^+)$ is the total width of the B_c^+ . Substituting Eq. (3) into the above equation and we have:

$$\begin{aligned} \left(\frac{\sigma(\mu)}{\mu}\right)^2 &= \left(\frac{\sigma(\mathcal{B}(Z \rightarrow B_c^\pm X))}{\mathcal{B}(Z \rightarrow B_c^\pm X)}\right)^2 + 4 \left(\frac{\sigma(|V_{cb}|)}{|V_{cb}|}\right)^2 + \\ &4 \left(\frac{\sigma(f_{B_c})}{f_{B_c}}\right)^2 + \left(\frac{\sigma(\Gamma(B_c^+))}{\Gamma(B_c^+)}\right)^2 + \text{Cov.} + \mathcal{O}(10^{-6}) \end{aligned} \quad (14)$$

where Cov. refers to the covariances between variables. The $\sigma(f_{B_c})/f_{B_c}$ and $\sigma(\Gamma(B_c^+))/\Gamma(B_c^+)$ are both at $\mathcal{O}(1\%)$ level. Sect. 4 shows that $\sigma(\mu)/\mu$ is also likely at 1% level at Tera-Z. This leaves the error terms to be dominated by the B_c^+ production term, which has a much bigger uncertainty, and will determine the uncertainty of $|V_{cb}|$. If the B_c^+ production term can be determined to $\mathcal{O}(1\%)$ level in the future and the covariances are also around the same level or less, the $|V_{cb}|$ could be determined to $\mathcal{O}(1\%)$ level as well.

3 Detector, software and the sample

The CEPC CDR (conceptual design report) [9] provides a detailed description of the detector setup and the software infras-

tructure. Both of them are inspired by the International Large Detector (ILD) of the International Linear Collider (ILC) and offer comparable performances. The general flow of software is as follows: 1) create simulated event samples using Pythia [21] and Whizard [22], 2) the MokkaPlus [23], a GEANT4 [24] based simulation tool, simulates the interaction with the detector, 3) the reconstruction framework mimics the electronics' responses and employ Arbor [25] and LICH [26] for physics object creation and lepton identification. Upon completing the standard procedures, two more software are used for further analysis. One is the LCFIPlus [27], an ILC software which can perform jet clustering and flavor tagging operations to separate different quark flavors in $Z \rightarrow q\bar{q}$. The other one is the TMVA [28], a multi-variable analysis tool for BDT (boosted decision tree) training.

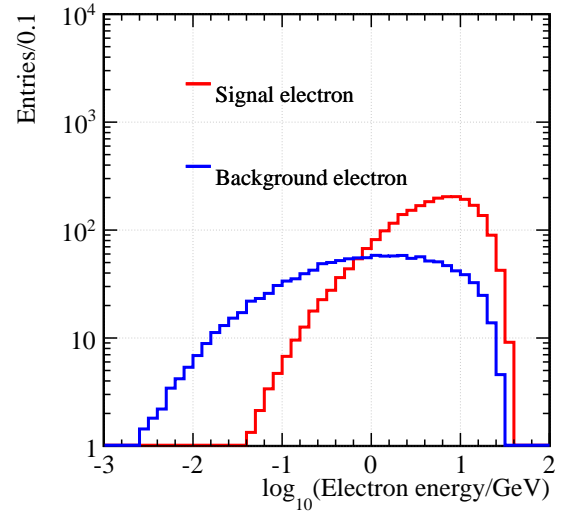


Fig. 5: Electron energy distribution in $B_c \rightarrow \tau \nu_\tau, \tau \rightarrow e \nu_\tau$.

The simulated sample consists of $Z \rightarrow q\bar{q}, B^+ \rightarrow \tau^+ \nu_\tau$ and $B_c^+ \rightarrow \tau^+ \nu_\tau$. The latter two are additional $Z \rightarrow q\bar{q}$ events that contain the corresponding processes. In order to save time, only a fraction of the $q\bar{q}$ (do not include $B_c^+/B^+ \rightarrow \tau^+ \nu_\tau$) events that are sufficient for analysis are actually simulated. The data are then scaled to reach the sample size corresponds to 10^9 Z boson decays. For the $B_c^+/B^+ \rightarrow \tau^+ \nu_\tau$, we simulated one million events each, and the final numbers and histograms are correspondingly scaled down. All of the scaling factors are shown in Table 1 and Table 2.

Since we are looking for leptonic final states, it is elucidating to demonstrate the lepton identification performance of CEPC. Figure 5 shows the generated energy spectrum of the signal and background electrons from $1.76 \times 10^5 B_c^+ \rightarrow \tau^+ \nu_\tau, \tau^+ \rightarrow e^+ \nu_e \bar{\nu}_\tau$ events (corresponds to one million $B_c^+ \rightarrow \tau^+ \nu_\tau$ events based on the $\mathcal{B}(\tau^+ \rightarrow e^+ \nu_e \bar{\nu}_\tau)$). The histograms are scaled down to match $1.3 \times 10^4 B_c^+ \rightarrow \tau^+ \nu_\tau$ events.). The signal electrons are the ones from $B_c^+ \rightarrow \tau^+ \nu_\tau, \tau^+ \rightarrow e^+ \nu_e \bar{\nu}_\tau$. We define the efficiency as the fraction of correctly identified electrons with respect to the total number of electrons. And the electron misidentification rate is defined as the rate of hadrons to be identi-

fied as electrons³. The overall lepton identification efficiency and mis-identification rate at energy above 2 GeV are better than 95% and 1%, respectively. For more details, see [26].

4 Analysis method and results

4.1 Analysis method

The characteristic event topology of $B_c^+/B^+ \rightarrow \tau^+ \nu_\tau, \tau^+ \rightarrow e^+/\mu^+ \nu \bar{\nu}$ in $Z \rightarrow b\bar{b}$ is shown in Fig. 6. The event can be divided into two hemispheres by the plane normal to the thrust. The thrust is the unit vector \hat{n} which maximizes

$$T = \frac{\sum_i |\mathbf{p}_i \cdot \hat{n}|}{\sum_i |\mathbf{p}_i|}, \quad (15)$$

where \mathbf{p}_i is the momentum of the i^{th} final state particle. We let the thrust point towards the hemisphere with less total energy. The axis where the thrust lies is the thrust axis. The hemisphere in which the $B_c^+/B^+ \rightarrow \tau^+ \nu_\tau, \tau^+ \rightarrow e^+/\mu^+ \nu \bar{\nu}$ decay occurs is the signal hemisphere and the other one is the tag hemisphere. The main event topology features are: 1) a b-jet in the tag hemisphere, 2) a single energetic e or μ with relatively large impact parameter along the thrust axis, 3) large energy imbalance between the signal and the tag hemisphere due to missing neutrinos in the signal hemisphere, 4) some soft fragmentation tracks are also present in both hemispheres. Based on the above definitions and features, it is clear that the thrust axis will mostly point towards the signal hemisphere. And the impact parameter is defined as follows: find the point on the thrust axis that is closest to the track, the impact parameter is the signed distance from this point to the interaction point. If the point lies in the signal hemisphere, then the impact parameter is positive, otherwise it is negative. Therefore, the signal lepton's impact parameter characterizes the sum of the decay length of the B meson and the τ . The main difference between B^+ and B_c^+ events is the impact parameter due to the difference between their lifetimes. The general analysis strategy is:

1. Employ a cut chain which exploits the main features of the event topology to reduce most of the backgrounds from Z decays to light flavor jets.

2. Use a BDT to separate jets with $B_c^+/B^+ \rightarrow \tau^+ \nu_\tau, \tau^+ \rightarrow e^+/\mu^+ \nu \bar{\nu}$ from other heavy flavor jets. In this case both the B_c and B events are considered as signal.

3. Use another BDT to separate the B_c events from the B and the remaining $b\bar{b}$ events.

Using two BDTs allows us to maximize the separation power of the final state lepton's impact parameter in the second BDT where it will be used as an additional parameter. We begin with the electron final state and later apply the same method to the muon final state as they are highly similar. The first stage cut chain is described in the following:

1. The b-tagging score (ranging from zero to unity) has to be greater than 0.6. This reduces most of non- $b\bar{b}$ $q\bar{q}$ backgrounds.

³ There is very little cross contamination between electron and muon

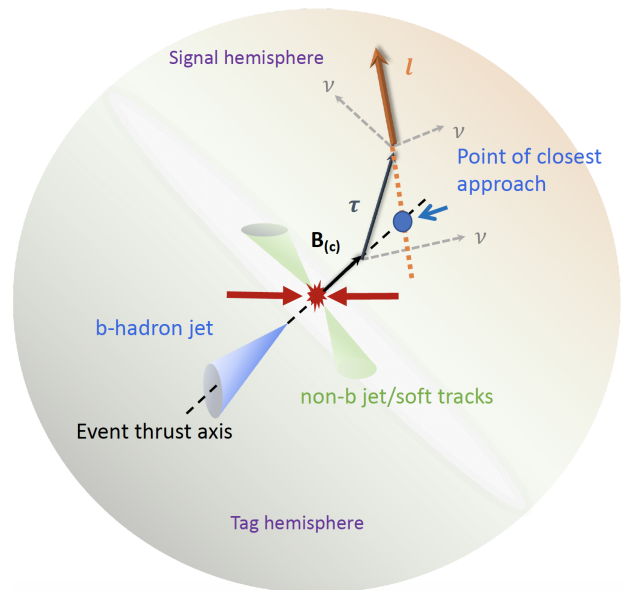


Fig. 6: $B_c/B \rightarrow \tau \nu, \tau \rightarrow e/\mu \nu \bar{\nu}$ in $Z \rightarrow b\bar{b}$ event topology. Be reminded that the extension of the lepton track passes close by the thrust axis, but does not need to intersect it.

2. The energy asymmetry, defined as the total energy in the tag hemisphere subtracted by the total energy in the signal hemisphere, has to be larger than 10 GeV. This step significantly reduces all of $q\bar{q}$ events again while preserving most of the B^+/B_c^+ events.

3. The signal hemisphere needs to have at least one electron. In case of multiple electrons, the most energetic one is selected for analysis. Most of the signal electrons have sufficient momenta to hit the electromagnetic calorimeter and meet the requirement.

4. The electron is the most energetic particle in the signal hemisphere.

5. The nominal B meson energy is greater than 20 GeV. The quantity is defined as:

$$E_B = 91.2 \text{ GeV} - \text{all visible energy except the signal electron.}$$

Table 1 shows the number of events during the cut chain. We have eliminated most of the light flavor backgrounds. Although their total number is comparable to the signal, considering the corresponding scale factors, they are likely to be eliminated by the following process, hence we ignore the events onwards.

After the first stage cut chain, we choose several variables for the BDT to eliminate $b\bar{b}$ and $c\bar{c}$ backgrounds. Some of the variables have been used in the L3 analysis [11]. They are listed as following:

- Nominal B meson energy.
- Maximum neutral cluster energy inside a 30 degree cone around the thrust axis in the signal hemisphere.
- The largest impact parameter along the thrust axis in the signal hemisphere besides the selected electron. After the cut chain, in most events the signal electron has the largest impact parameter in the signal hemisphere.

Table 1: The cut chain for the electron final state for 10^9 Z bosons. The numbers in the parentheses are corresponding scale factors. In the final row, the numbers with stars mean the corresponding channels are not used in the second BDT training in order to avoid possible overfitting. Instead, we make a conservative assumption that all of the events passed the first BDT cut survive the second BDT cut.

	$B_c^\pm \rightarrow \tau \nu_\tau(0.013)$		$B^\pm \rightarrow \tau \nu_\tau(0.013)$		$d\bar{d}(15) + u\bar{u}(12) + s\bar{s}(15)$	$c\bar{c}(4.8)$	$b\bar{b}(3.25)$
	$\tau \rightarrow e \nu \bar{\nu}$	excl. $\tau \rightarrow e \nu \bar{\nu}$	$\tau \rightarrow e \nu \bar{\nu}$	excl. $\tau \rightarrow e \nu \bar{\nu}$			
All events	2,303	10,691	2,270	10,633	419,928,342	119,954,033	151,286,603
b-tag > 0.6	1,611	7,463	1,547	7,151	2,134,617	7,344,014	116,723,067
Energy asymmetry > 10 GeV	1,425	6,184	1,389	5,801	486,762	1,609,771	30,064,030
Has electron in signal hemisphere	1,273	1,300	1,243	1,132	143,595	625,670	15,905,613
Electron is the most energetic particle	915	116	859	93	8,490	79,190	4,587,248
$E_B > 20$ GeV	909	112	852	88	981	34,147	3,203,073
1 st BDT score > 0.99	390	12	259	4	—	48	910
2 nd BDT score > 0.4	199	12*	73	4*	—	48*	33

- Energy asymmetry.
- Second largest track momentum in the signal hemisphere.
- Electron’s energy.
- Electron’s impact parameter along the thrust axis.

We then apply cuts on the outputs of two BDTs as described before. In the first BDT, we use all but the electron’s impact parameter along the thrust axis. The parameter will then be added in the second BDT.

4.2 Results

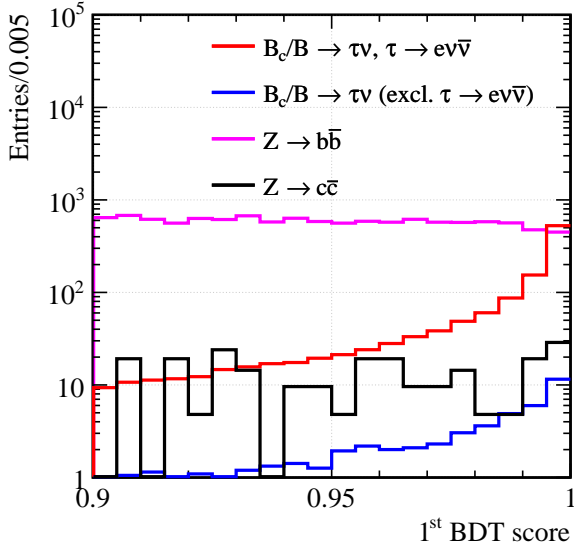


Fig. 7: The first BDT score. Here the notation B_c/B means the combination of the two data.

The first BDT scores are shown in Fig. 7. They range from -1 to 1, of which we showed the rightmost part in the figure.

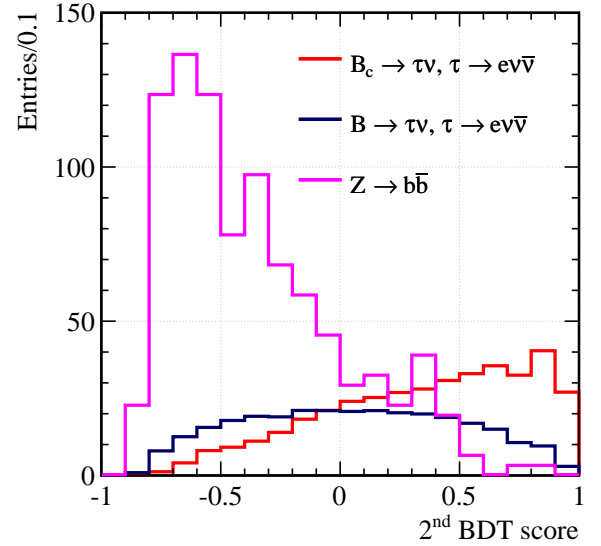


Fig. 8: The second BDT score.

The presence of the signal is apparent at large BDT scores. We apply a cut on the BDT score at 0.99 and only use $B_c/B \rightarrow \tau \nu_\tau, \tau \rightarrow e \nu \bar{\nu}$ and $Z \rightarrow b\bar{b}$ for the second BDT. Ignoring the non-electron τ decay and $Z \rightarrow c\bar{c}$ channels will avoid the possibility of overfitting attributed to these channels, besides the numbers are already small anyway. Then we make a conservative assumption that all of the ignored events survive the second BDT cut, except the light flavor events. The second BDT scores are shown in Fig. 8 and we cut at 0.4. The cut on the BDT scores are chosen to maximize the final signal strength accurately. Numbers from two BDT results are shown in Table 1.

Now we can compute the relative accuracy of the signal strength:

$$\sigma(\mu)/\mu = \sqrt{N_S + N_B}/N_S, \quad (16)$$

Table 2: The cut chain for the muon final state for 10^9 Z bosons. The numbers in the parentheses and the star at the final row have the same meaning as in Table 1.

	$B_c^\pm \rightarrow \tau \nu_\tau(0.013)$		$B^\pm \rightarrow \tau \nu_\tau(0.013)$		$d\bar{d}(15) + u\bar{u}(12) + s\bar{s}(15)$	$c\bar{c}(4.8)$	$b\bar{b}(3.25)$
	$\tau \rightarrow \mu \nu \bar{\nu}$	excl. $\tau \rightarrow \mu \nu \bar{\nu}$	$\tau \rightarrow \mu \nu \bar{\nu}$	excl. $\tau \rightarrow \mu \nu \bar{\nu}$			
All events	2,250	10,745	2,213	10,698	419,928,342	119,954,033	151,286,603
b-tag > 0.6	1,576	7,499	1,505	7,199	2,134,617	7,344,014	116,723,067
Energy asymmetry > 10 GeV	1,387	6,222	1,348	5,848	486,762	1,609,771	30,064,030
Has Muon in signal hemisphere	1,175	2,204	1,168	2,233	244,752	813,083	19,569,212
Muon is the most energetic particle	882	222	838	171	9,777	89,290	4,943,760
$E_B > 20$ GeV	877	216	832	166	1,713	39,583	3,516,717
1 st BDT score > 0.99	394	48	306	28	—	76	1,125
2 nd BDT score > 0.4	192	13	68	5	—	76*	59

where N_S and N_B denote the number of signal and background events that pass all selection cuts, respectively. For the electron final states, we have $\sigma(\mu_e)/\mu_e = 9.7\%$. We can repeat the entire process for the muon final state. Here we will include the non-muon τ decay channels in the second BDT since the numbers of events are significantly larger. The results are shown in Table 2, and $\sigma(\mu_\mu)/\mu_\mu = 10.6\%$. Combining the two final states, we have $\sigma(\mu)/\mu = 7.2\%$. It is now straightforward to calculate the $\sigma(\mu)/\mu$ for both $B_c^+/B^+ \rightarrow \tau^+ \nu_\tau$ at Tera-Z at various $R_{B_c/B}$. For the $B \rightarrow \tau \nu, \tau \rightarrow e/\mu \nu \bar{\nu}$ analysis, all we need to do is repeating the second BDT after switching the signal and background status between it and the B_c . Figure 9 shows their relationship with $R_{B_c/B}$. Here, the yield $N(B^\pm \rightarrow \tau^+ \nu_\tau)$ is fixed at 1.3×10^4 per one billion Z. The projected $\sigma(\mu)/\mu$ s at Tera-Z are around $\mathcal{O}(0.1) \sim \mathcal{O}(1)\%$ level for both $B_c^+ \rightarrow \tau^+ \nu_\tau$ and $B^+ \rightarrow \tau^+ \nu_\tau$. At the $R_{B_c/B}$ value given in Eq. (2), where the yield $N(B_c^\pm \rightarrow \tau^+ \nu_\tau)$ is around 3.6×10^3 per one billion Z, we need around 10^9 Z boson decays to achieve five σ significance. In Sect. 2 we have discussed the $|V_{cb}|$ measurement and with current results we argue that the accuracy could reach up to $\mathcal{O}(1)\%$ level with certain improvements.

4.3 Phenomenological Impact on New Physics

As we have shown in Sec. 2, based on the current results on NP in $b \rightarrow c \tau \nu$, the $\Gamma(B_c^+ \rightarrow \tau^+ \nu_\tau)$ tends to deviate from SM predictions, but the statistical importance is not significant. From Fig. 9, one can see that at CEPC the $\sigma(\mu)/\mu$ for $B_c^+ \rightarrow \tau^+ \nu_\tau$ can reach about 1% level. This includes the constraint in both the production of B_c^+ and the decay into $\tau^+ \nu_\tau$. If the production mechanism is well understood, the result on $\sigma(\mu)/\mu$ would also imply that the uncertainties in $\Gamma(B_c^+ \rightarrow \tau^+ \nu_\tau)$ are reduced to the percent level. On the other side, in the future one can also use the $\mathcal{B}(B_c^+ \rightarrow J/\psi \pi^+)$ as a calibration mode. In theory the Lattice QCD can calculate the $B_c \rightarrow J/\psi$ transition form factors while the perturbative contributions are well under control in perturbation theory.

One can use such results on $\Gamma(B_c^+ \rightarrow \tau^+ \nu_\tau)$ to probe NP to a high precision. In Fig. 10, we show the constraints on $\text{Re}[C_{V_2}]$ and $\text{Im}[C_{V_2}]$. If the central values in Eq. (9) remain the same while the uncertainty in $\Gamma(B_c^+ \rightarrow \tau^+ \nu_\tau)$ is reduced to 1%, the

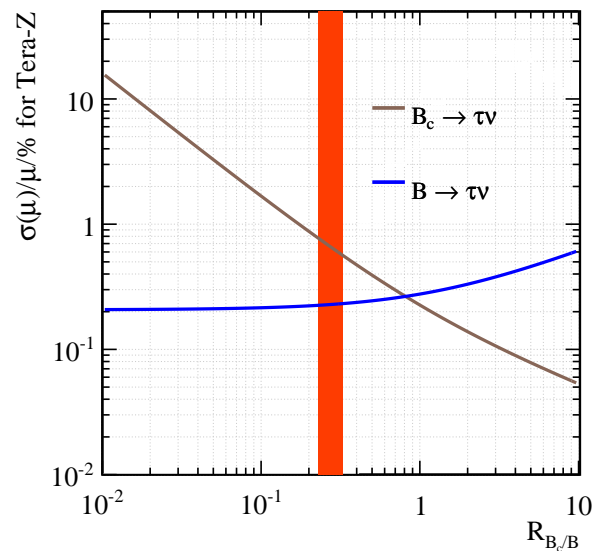


Fig. 9: $\sigma(\mu)/\mu$ at Tera-Z versus $R_{B_c/B}$. The estimated range of $R_{B_c/B}$ in Eq. (2) is shown in red band. Be reminded that the actual uncertainty is larger since we lack uncertainty for $\mathcal{B}(Z \rightarrow B_c^\pm X)$.

allowed region for C_{V_2} shrinks as the dark-blue region, where the deviation from the SM is greatly enhanced.

Similar results can be obtained for NP coefficients C_{S_1} and C_{S_2} , but as we have demonstrated in Sec. 2, both scenarios will induce dramatic changes to $\Gamma(B_c^+ \rightarrow \tau^+ \nu_\tau)$. These NP effects are so large that they would already be verified or ruled out before entering into the very precision era of the CEPC. Thus it is less meaningful to present the constraints for these two coefficients.

5 Conclusion

Nowadays hunting for new physics beyond the Standard Model is a primary objective in particle physics. In this paper, we have

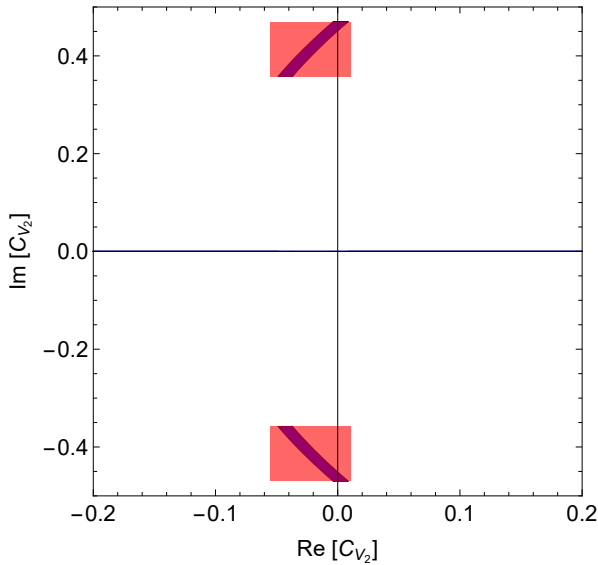


Fig. 10: Constraints on the real and imaginary parts of C_{V_2} . The red shaded area corresponds to the current constraints using available data on $b \rightarrow c \tau \nu$ decays. If the central values in Eq. (9) remain while the uncertainty in $\Gamma(B_c^+ \rightarrow \tau^+ \nu_\tau)$ is reduced to 1%, the allowed region for C_{V_2} shrinks to the dark-blue region.

first demonstrated that the decay $B_c^+ \rightarrow \tau^+ \nu_\tau$ provides a unique opportunity to probe new physics contributions especially to the (pseudo)scalar interactions that exist in many popular models like the two Higgs doublet model and the leptoquark models.

We then analyzed the decay $B_c^+ \rightarrow \tau^+ \nu_\tau, \tau^+ \rightarrow e^+/\mu^+ \nu_{\bar{e}}/\nu_{\bar{\mu}}$ at the CEPC Z pole. We took references of the methods used in the L3 analysis [11] on the search of $B^+ \rightarrow \tau^+ \nu_\tau$, which shares a similar event topology. The backgrounds under consideration are $Z \rightarrow q\bar{q}, B^+ \rightarrow \tau^+ \nu_\tau$ as well as other τ decay channels of $B_c^+ \rightarrow \tau^+ \nu_\tau$. We used a first stage cut chain to suppress most of the light-flavor backgrounds, and subsequently used 2-stage BDT method to perform a fine-tuned multi-variable analysis. The first BDT separates heavy flavor backgrounds and the second BDT separates $B^+ \rightarrow \tau^+ \nu_\tau$ events. The current detector design and reconstruction algorithms provide excellent signal lepton reconstruction efficiency and purity, and do not pose significant constraints on the analysis. We have demonstrated that under current estimates for $N(B_c^\pm \rightarrow \tau^\pm \nu_\tau)$ of around 3.6×10^3 per one billion Z, we need around $\sim 10^9$ Z decays to achieve five σ significance. The relative accuracy of signal strength could reach around 1% level at Tera-Z. If the total B_c^+ yield can be determined to $\mathcal{O}(1\%)$ level accuracy in the future the $|V_{cb}|$ can also be expected to be measured to $\mathcal{O}(1\%)$ level of accuracy. Our theoretical analysis shows the channel has a good potential for NP search and could provide a significant constraint on the NP related to the Wilson coefficient C_{V_2} in Eq. (5). We also showed the projected signal strength accuracy for various signal event numbers for both $B_c^+/B^+ \rightarrow \tau^+ \nu_\tau$. The results could be improved with a more exhaustive analysis, es-

pecially the inclusion of hadronic τ decays and a larger sample of MC-simulated events.

To summarize, we have demonstrated the CEPC's benchmark capability on the $B_c^+ \rightarrow \tau^+ \nu_\tau$ study. The results show the CEPC could provide a new opportunity to search for the NP such as the 2HDM and LQ models, measure $|V_{cb}|$ and test our understanding of QCD.

Acknowledgement

We thank Yiming Li, Haibo Li and Jianchun Wang for useful discussions, and Chengdong Fu and Gang Li for providing some of the samples and tools. We give special thank to Fefen An for some preliminary studies and useful discussions. This work is supported by the Beijing Municipal Science & Technology Commission, project No. Z181100004218003 and Z191100007219010, the Natural Science Foundation of China under grant No. 11735010, 11911530088, 11775110, and 11690034, the Natural Science Foundation of Shanghai under grant No. 15DZ2272100, the DFG Emmy-Noether Grant No. BE 6075/1-1. We also acknowledge the Priority Academic Program Development for Jiangsu Higher Education Institutions (PAPD).

References

1. F. Abe *et al.* [CDF], Phys. Rev. Lett. **81**, 2432-2437 (1998) doi:10.1103/PhysRevLett.81.2432 [arXiv:hep-ex/9805034 [hep-ex]].
2. F. Abe *et al.* [CDF], Phys. Rev. D **58**, 112004 (1998) doi:10.1103/PhysRevD.58.112004 [arXiv:hep-ex/9804014 [hep-ex]].
3. P.A. Zyla *et al.* (Particle Data Group), to be published in Prog. Theor. Exp. Phys. 2020, 083C01 (2020).
4. J. Lees *et al.* [BaBar], Phys. Rev. Lett. **109** (2012), 101802 doi:10.1103/PhysRevLett.109.101802 [arXiv:1205.5442 [hep-ex]].
5. A. Abdesselam *et al.* [Belle], [arXiv:1904.08794 [hep-ex]].
6. R. Aaij *et al.* [LHCb], Phys. Rev. Lett. **120** (2018), 171802 doi:10.1103/PhysRevLett.120.171802 [arXiv:1708.08856 [hep-ex]].
7. X. Q. Li, Y. D. Yang and X. Zhang, JHEP **08**, 054 (2016) doi:10.1007/JHEP08(2016)054 [arXiv:1605.09308 [hep-ph]].
8. R. Alonso, B. Grinstein and J. M. Camalich, Phys. Rev. Lett. **118**, 081802 (2017) doi:10.1103/PhysRevLett.118.081802 [arXiv:1611.06676 [hep-ph]].
9. CEPC Study Group, [arXiv:1811.10545 [hep-ex]].
10. Line Shape Sub-Group of the LEP Electroweak Working Group, DELPHI, LEP, ALEPH, OPAL, L3 Collaboration, Combination procedure for the precise determination of Z boson parameters from results of the LEP experiments, [arXiv:hep-ex/0101027[hep-ex]].
11. M. Acciarri *et al.* [L3], Phys. Lett. B **396**, 327-337 (1997) doi:10.1016/S0370-2693(97)00138-X
12. M. L. Mangano and S. Slabospitsky, Phys. Lett. B **410**, 299-303 (1997) doi:10.1016/S0370-2693(97)00953-2 [arXiv:hep-ph/9707248 [hep-ph]].

13. A. Akeroyd, C. H. Chen and S. Recksiegel, Phys. Rev. D **77**, 115018 (2008) doi:10.1103/PhysRevD.77.115018 [arXiv:0803.3517 [hep-ph]].
14. J. Jiang, L. B. Chen and C. F. Qiao, Phys. Rev. D **91**, 034033 (2015) doi:10.1103/PhysRevD.91.034033 [arXiv:1501.00338 [hep-ph]].
15. B. Colquhoun *et al.* [HPQCD], Phys. Rev. D **91** (2015), 114509 doi:10.1103/PhysRevD.91.114509 [arXiv:1503.05762 [hep-lat]].
16. V. V. Kiselev, A. E. Kovalsky, A. K. Likhoded, Nucl. Phys. B **585** (2000) 353-382 doi:10.1016/S0550-3213(00)00386-2 [arXiv:hep-ph/0002127[hep-ph]].
17. J. Kalinowski, Phys. Lett. B **245** (1990) 201-206, doi:10.1016/0370-2693(90)90134-R.
18. W. S. Hou, Phys. Rev. D **48**, 2342 (1993). doi:10.1103/PhysRevD.48.2342
19. Z. R. Huang, Y. Li, C. D. Lu, M. A. Paracha and C. Wang, Phys. Rev. D **98** (2018), 095018 doi:10.1103/PhysRevD.98.095018 [arXiv:1808.03565 [hep-ph]].
20. K. Cheung, Z. R. Huang, H. D. Li, C. D. Lü, Y. N. Mao and R. Y. Tang, [arXiv:2002.07272 [hep-ph]].
21. The Pythia Group, An Introduction to PYTHIA 8.2, Comput. Phys. Commun. **191** (2015).
22. W. Kilian, T. Ohl, J. Reuter, WHIZARD: simulating multi-particle processes at LHC and ILC, Eur. Phys. J. C **71**, 1742 (2011).
23. C.D. Fu, Full simulation software at CEPC, <http://cepcdoc.ihep.ac.cn/DocDB/0001/000167/001>, Accessed 23 Oct 2017.
24. S. Agostinelli *et al.*, Geant4-a simulation toolkit. Nucl. Instrum. Methods Phys. Res. Sect. A Accel. Spectrom. Detect. Assoc. Equip. **506**, 250–303 (2003)
25. M.Q. Ruan *et al.*, Reconstruction of physics objects at the Circular Electron Positron Collider with Arbor, Eur. Phys. J. C **78**, 426 (2018).
26. D. Yu *et al.*, Eur. Phys. J. C **77** (2017) 591 [arXiv:1701.07542].
27. T. Suehara, T. Tanabe, LCFIPlus: A framework for jet analysis in linear collider studies, Nuclear Instruments and Methods in Physics Research Section A: Accelerators, Spectrometers, Detectors and Associated Equipment, February, 2016.
28. A. Hocker *et al.*, TMVA-toolkit for multivariate data analysis, physics/0703039, CERN-OPEN-2007-007